

## Refinement of the substructure and superstructure of romanechite

SHIRLEY TURNER,\* JEFFREY E. POST

Department of Mineral Sciences, Smithsonian Institution, Washington, D.C. 20560, U.S.A.

### ABSTRACT

The substructure and superstructure of romanechite,  $(\text{Ba}, \text{H}_2\text{O})_2\text{Mn}_5\text{O}_{10}$ , were refined using a crystal from Schneeberg, Germany. The subcell is monoclinic, space group  $C2/m$ , with  $a = 13.929(1) \text{ \AA}$ ,  $b = 2.8459(4) \text{ \AA}$ ,  $c = 9.678(1) \text{ \AA}$ ,  $\beta = 92.39(1)^\circ$ ,  $Z = 2$ , and it refined to  $R = 0.036$  for anisotropic temperature factors using 598 reflections. The Mn(2) octahedra of the structure show significant distortion consistent with the concentration of  $\text{Mn}^{3+}$  on the Mn(2) site.

The supercell, consisting of a tripling along  $b$  (i.e., the tunnel axis), results from ordering of Ba and  $\text{H}_2\text{O}$  along the tunnel lengths. Further, long-exposure diffraction patterns show modulated streaks along  $[20\bar{1}]^*$ , implying only short-range ordering between the tunnels in one direction. A simplest monoclinic unit cell was chosen with space group  $C2/m$  and  $Z = 6$ . It was refined to  $R = 0.041$  for anisotropic temperature factors using 954 reflections. Ba preferentially occupies the Ba(1) site, and correspondingly the closest framework octahedra [Mn(2) site] are preferentially occupied by  $\text{Mn}^{3+}$ .

### INTRODUCTION

Romanechite,  $(\text{Ba}, \text{H}_2\text{O})_2\text{Mn}_5\text{O}_{10}$ , is one of several naturally occurring manganese oxides with a tunnel structure. Its structure is closely related to those of hollandite and todorokite and to their many derivative structures (Turner and Buseck, 1981). Romanechite rarely occurs as sizable single crystals but is intergrown with other minerals, commonly at the unit-cell level (Turner and Buseck, 1979; Giovanoli and Balmer, 1983). Its occurrence in mixtures has led to confusion in nomenclature. The mineral has been called psilomelane in the past; psilomelane is now a term reserved for a mixture of manganese oxide minerals, and romanechite refers to a particular manganese mineral.

The romanechite structure was solved by Wadsley (1953) in two dimensions using Weissenberg film data ( $R$  value = 0.16). Wadsley showed that the romanechite structure consists of double and triple chains of edge-sharing Mn-O octahedra that share corners to produce a framework containing large rectangular-shaped tunnels measuring two by three  $[2 \times 3]$  octahedra on an edge (Fig. 1). The tunnels are occupied by  $\text{Ba}^{2+}$  (and minor amounts of other cations, e.g.,  $\text{Na}^+$ ,  $\text{K}^+$ ,  $\text{Sr}^{2+}$ , etc.) and  $\text{H}_2\text{O}$ , and the charges of the tunnel cations are offset by substitution of lower-valence cations in the octahedral sites. By comparison, the hollandite structure is constructed of double octahedral chains and todorokite of triple chains resulting in frameworks with  $[2 \times 2]$  and  $[3 \times 3]$  square tunnels, respectively.

Two aspects of the romanechite structure have been of particular interest. First, there has been a question as to

the location and nature of the lower-valence Mn cations. On the basis of approximate bond distances obtained by Wadsley (1953), Burns et al. (1983) proposed that the lower-valence Mn is segregated into the Mn sites at the edges of the triple chains of romanechite. Burns et al. (1983) also proposed a similar segregation in the analogous sites of todorokite. Recently, such an ordering of lower-valence Mn was found for a related material ( $\text{Rb}_{0.27}\text{MnO}_2$ ) with a  $2 \times 5$  structure (Tamada and Yamamoto, 1986). Structure refinements of some hollandite structures and  $\text{Rb}_{0.27}\text{MnO}_2$  indicate that the lower-valence Mn cation is  $\text{Mn}^{3+}$  rather than  $\text{Mn}^{2+}$  (Post et al., 1982; Tamada and Yamamoto, 1986); size consideration and exchange experiments led Giovanoli and Balmer (1983) to the same conclusion, corroborating earlier work of Yanchuk (1973) and Yanchuk and Povarennykh (1975). Second, Wadsley (1953) proposed the existence of a superstructure resulting from ordering of the tunnel cations and water. Recently, the presence of such a superstructure was confirmed by electron diffraction (Chukhrov et al., 1983). These aspects of the romanechite structure are further explored in this paper.

### EXPERIMENTAL DETAILS

The romanechite sample chosen for study is from Schneeberg, Germany (USNM no. C1818). The locality is also the source of the crystal studied by Wadsley (1953) and is apparently unique as an occurrence of romanechite crystals suitable for single-crystal X-ray study. The bulk of the specimen from which the crystal was obtained is botryoidal in appearance with crystals scattered on the surfaces. Many crystals were examined by precession and Weissenberg methods in order to choose one suitable for structure analysis. The crystal chosen for data collection showed some streaking of spots indicating a rotation of about  $5^\circ$  around the  $b$  axis. The wedge-shaped crystal has approximate dimensions of

\* Present address: Center for Analytical Chemistry, National Bureau of Standards, Gaithersburg, Maryland 20899, U.S.A.

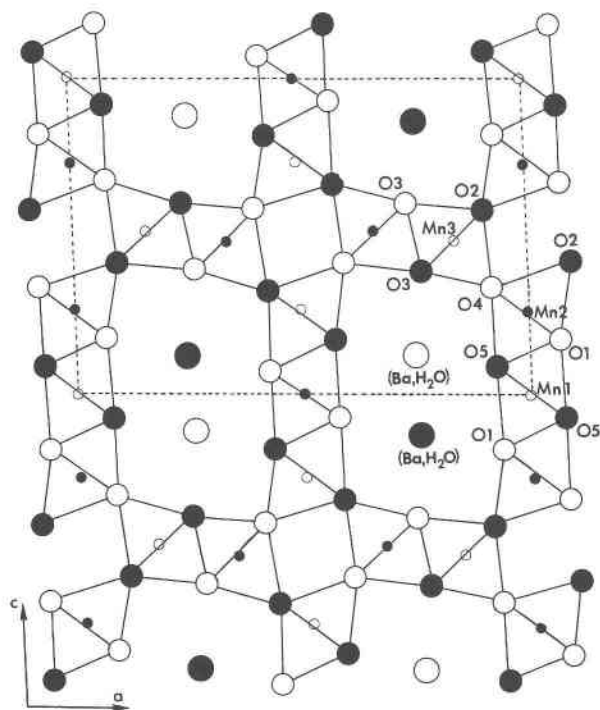
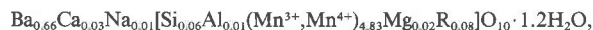


Fig. 1. Projection down  $b$  of the romanechite substructure. Open circles indicate  $y = 0$ , filled circles indicate  $y = 1/2$ .

150  $\mu\text{m}$  ( $\parallel a$ )  $\times$  100  $\mu\text{m}$  ( $\parallel b$ )  $\times$  70  $\mu\text{m}$  ( $\parallel c$ ), and it has irregular and stepped surfaces.

Electron-microprobe analyses of the bulk of the Schneeberg sample indicate an average formula of



where R = W, Cu, Zn, Ni, and Co. Water analyses were performed by the Penfield method. The analysis is in good agreement with previously reported values for romanechites from this locality. Unit-cell dimensions (Table 1) were determined from X-ray powder-diffraction data obtained from the bulk Schneeberg sample using Rietveld refinement methods (Post and Bish, in prep.) using all reflections from  $25^\circ$  to  $110^\circ$   $2\theta$  ( $\text{CuK}\alpha$  radiation). The presence of a supercell was evident from weak reflections on long-exposure ( $>60$  h) precession and oscillation diffraction patterns (Figs. 2a, 2b). These patterns confirm the tripling along  $b^*$  reported by Chukhrov et al. (1983) and contradict the doubling along  $b^*$  reported by Mukherjee (1965). Figure 2b reveals that the superstructure "spots" are, in fact, streaks that are oriented in the  $[20\bar{1}]^*$  direction. These streaks are not continuous but are modulated perpendicular to  $c^*$ . The streaks have an additional shorter and weaker modulation along their lengths. The spacing of this weaker modulation corresponds to that of the subcell spots. A sketch of overall reciprocal space is shown in Figure 2c (the weaker modulation is not shown). For the data collection, a "simplest" supercell was assumed with  $b$  of the supercell triple that of the subcell. Intensity data were collected at points corresponding to the weak modulation of the streaks.

The X-ray intensity data were collected on a Krisel-automated Picker diffractometer using Nb-filtered  $\text{MoK}\alpha$  radiation. The supercell reflections were collected separately to allow a slower scan rate and longer background counts (collections parameters for the subcell and supercell are given in Table 1). Standard

TABLE 1. Crystal and structure-refinement data

	Subcell	Supercell
Space group	$C2/m$	$C2/m$
$a$ ( $\text{\AA}$ )	13.929(1)	13.929*
$b$ ( $\text{\AA}$ )	2.8459(4)	$2.8459 \times 3$
$c$ ( $\text{\AA}$ )	9.678(1)	9.678
$\beta$	$92.39(1)^\circ$	$92.39^\circ$
$Z$	2	6
$2\theta$ range	$3\text{--}60^\circ$	$3\text{--}50^\circ$
Scan speed	$0.75^\circ/\text{min}$	$0.5^\circ/\text{min}$
Background (s)	30	60
Data collected (relative to supercell)	$\pm h, k, \pm l$ for $k = 3n$	$\pm h, k, \pm l$ for $k \neq 3n$
Standard reflections	4	2
Time between standards (min)	180	240
Average difference between absorption-corrected equivalent reflections	7.40%	6.94%
Unique reflections	598	954
Parameters refined		
isotropic	30	68
anisotropic	60	143
$R$ factors		
isotropic	0.060	0.068
anisotropic	0.036	0.041

\* Cell parameters for supercell are those refined for subcell with  $b$  tripled.

reflections showed variations of less than 2% during both data collections. Only data with  $I \geq 2.5\sigma$  were used. Intensities were corrected for absorption using the analytical correction program of Burnham (1966). The average differences between equivalent reflections after the absorption correction for the sub- and supercells are fairly large (Table 1), possibly reflecting problems encountered in modeling the irregular shape of the crystal for the absorption correction.

## REFINEMENT

Refinements were carried out using the X-ray 76 package of Stewart (1976). Ionic scattering factors and anomalous dispersion corrections were taken from the *International Tables for X-ray Crystallography* (1974). Unit weights were used throughout the refinement.

Initial atom positions for the structure refinement were those of Wadsley (1953). The substructure was initially refined assuming only Ba in the mixed  $(\text{Ba}, \text{H}_2\text{O})$  tunnel sites. Least-squares, full-matrix refinement of atom positions and the Ba occupancy yielded  $R = 0.065$  using isotropic temperature factors and  $R = 0.041$  using anisotropic temperature factors. At this point, water was included in the refinement (as O), and the Ba occupancy was fixed at 0.33, as determined by microprobe analysis. The water [O(6)] occupancy refined to 0.59(4) [0.71(4) for anisotropic refinement], which agrees well with analytical values ( $\sim 0.6$ ) and the expected  $\sim 1:2$  ratio of  $\text{Ba}:\text{H}_2\text{O}$ . The  $R$  value improved to 0.060 and 0.036 for isotropic and anisotropic temperature factors, respectively. The low  $U_{22}$  anisotropic temperature factors (Table 2) for several atoms possibly reflect the difficulties encountered with the absorption correction. The relatively large thermal parameters for the  $(\text{Ba}, \text{H}_2\text{O})$  site probably result from a combination of thermal motion in the large tunnel site and possible positional disorder of the Ba and/or water

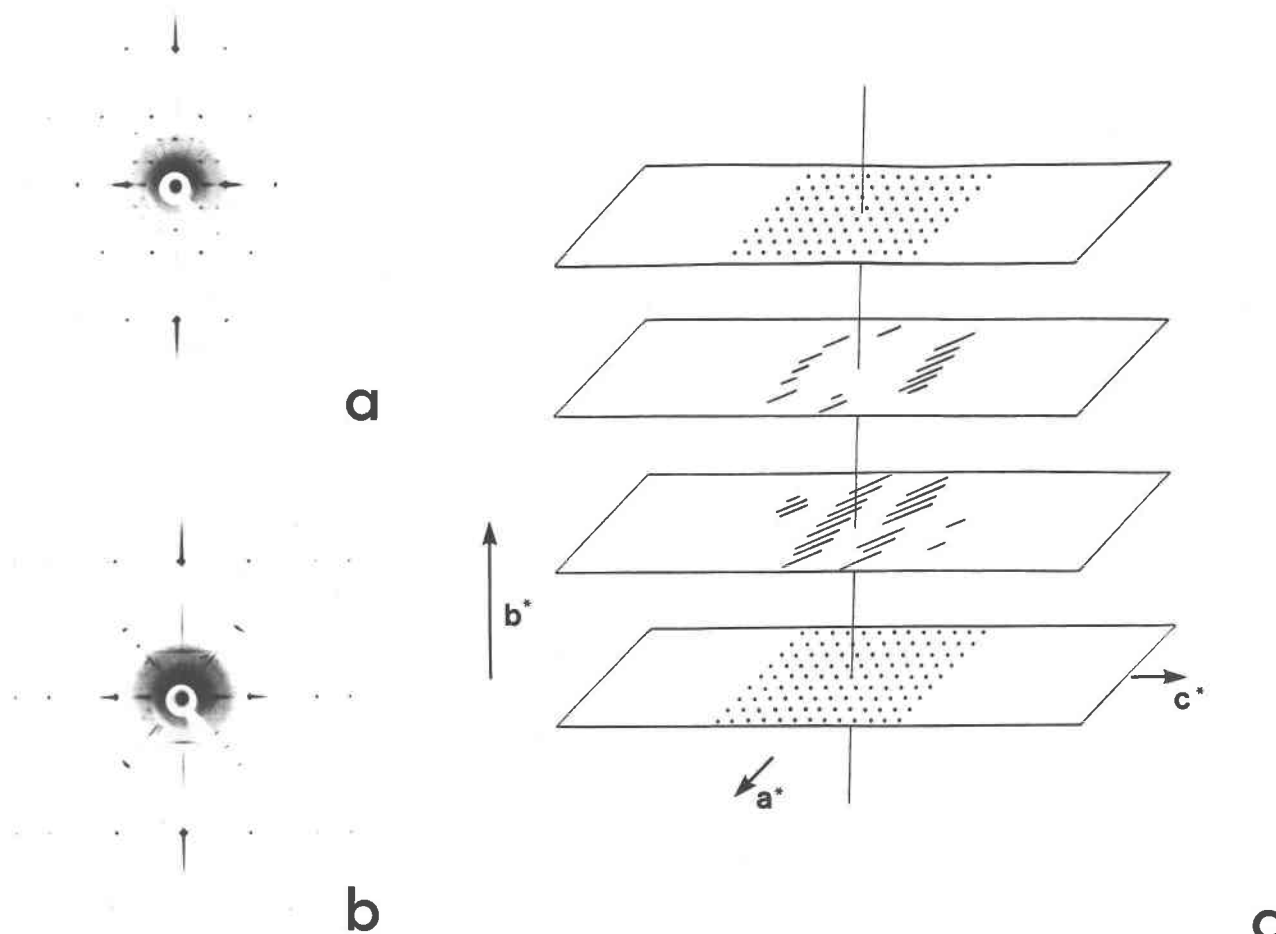


Fig. 2. Precession diffraction patterns and sketch of romanechite superstructure. (a) Pattern parallel to  $b^*$  showing tripling of subcell  $b^*$ . (b) Pattern  $90^\circ$  from pattern in (a) showing that the "spots" are actually modulated streaks (streaks are along  $[20\bar{1}]^*$ ). (c) Sketch of reciprocal lattice of the romanechite superstructure. The vertical scale (along  $b^*$ ) is exaggerated.

molecules. The observed and calculated structure factors are shown in Table 3.<sup>1</sup> Final atom positions, occupancies, and isotropic and anisotropic temperature factors for this refinement are given in Table 2, and the structure is plotted in Figure 1. Selected bond lengths are listed in Table 4.

The superstructure was refined by combining the subcell and supercell reflections. In the superstructure, there are two independent  $(\text{Ba}, \text{H}_2\text{O})$  sites and twice the number of Mn and O atoms in the asymmetrical unit as in the substructure. In the superstructure, O(11) and O(12) represent water molecules (Table 5). In order to reduce correlations arising from pseudosymmetry, before beginning the refinement, the framework-atom positions were randomly shifted slightly from those determined for the substructure. The refinement resulted in small but significant adjustments of the Mn and O positions. Major shifts,

however, occurred for the  $(\text{Ba}, \text{H}_2\text{O})$  site-occupancy factors. In the course of the refinement, the total Ba occupancy was constrained to the microprobe value, and the combined Ba and water occupancy was fixed to 1.0 for each tunnel site. The observed and calculated structure factors are given in Table 6 (see footnote 1); the refined superstructure-atom positions, isotropic and anisotropic temperature factors, and occupancies are given in Table 5; and selected bond lengths are given in Table 7.

## DISCUSSION

In general, our structure agrees well with that determined by Wadsley, although there are significant differences in atom positions and bond lengths. The greater precision of our refinement provides insights into some of the details of the romanechite structure.

### Lower-valence Mn

If there were no tunnel cations in the manganese oxide tunnel structures, their ideal formula would be  $\text{Mn}^{4+}\text{O}_2$ . The presence of tunnel cations means that some lower-

<sup>1</sup> Copies of Table 3 and Table 6 may be ordered as document AM-BB 385 from the Business Office, Mineralogical Society of America, 1625 I Street, N.W., Suite 414, Washington, D.C. 20006, U.S.A. Please remit \$5.00 in advance for the microfiche.

TABLE 2. Romanechite substructure atom positions, temperature factors, and occupancies

Atom	X	Y	Z	$U_{eq}^*$	Occ**	$U_{11}^\dagger$	$U_{22}^\dagger$	$U_{33}^\dagger$	$U_{12}^\dagger$	$U_{13}^\dagger$	$U_{23}^\dagger$
Mn(1)	0.0	0.5	0.0	75		181(8)	24(8)	97(7)	0	42(6)	0
Mn(2)	0.99978(9)	0	0.2682(1)	77		140(6)	35(5)	93(5)	0	10(4)	0
Mn(3)	0.3401(1)	0	0.4841(1)	81		139(5)	37(5)	102(5)	0	18(4)	0
O(1)	0.5669(4)	0	0.1773(6)	96		187(28)	35(26)	134(25)	0	37(21)	0
O(2)	0.0976(4)	0	0.4244(6)	104		188(28)	41(26)	144(25)	0	-12(21)	0
O(3)	0.7663(4)	0	0.3958(6)	101		168(27)	54(26)	114(24)	0	12(20)	0
O(4)	0.4248(4)	0	0.3354(6)	97		158(26)	43(26)	136(24)	0	44(20)	0
O(5)	0.9263(5)	0	0.0721(7)	147		222(32)	47(28)	303(34)	0	108(26)	0
Ba(1)	0.2466(1)	0	0.1242(3)	125	0.33‡	131(8)	119(15)	127(10)	0	9(6)	0
O(6)	0.250(2)	0	0.131(3)	125	0.59(4)§						

\*  $U_{eq} = (U_{11}U_{22}U_{33})^{1/3}$ .

\*\* Fraction per formula unit.

† The coefficients for anisotropic temperature factors are each  $\times 10^4$ .

‡ Fixed to microprobe value.

§ Occupancy for isotropic refinement [O(6) went nonpositive definite during anisotropic refinement, and occupancy factor increased to 0.71(4)].

valence cations must be present to maintain charge balance. The lower-valence Mn cations are larger than Mn<sup>4+</sup> and will therefore have larger average Mn–O bond distances. Specifically, the average Mn<sup>2+</sup>–O bond distance is 2.23 Å (Shannon, 1976) and the average Mn<sup>3+</sup>–O bond distance is 2.04 Å (Shannon, 1976), as compared to an average Mn<sup>4+</sup>–O bond distance of  $\sim 1.89$  Å derived for pyrolusite (Baur, 1976). In Table 8, the average octahedral bond lengths are summarized for various manganese oxide structures. From Wadsley's refinement, a larger average octahedral size is derived for the Mn(2) site although the bond distances are approximate (no error estimates). Our refinement of the substructure confirms that the Mn(2) octahedra are larger (Table 8). Further, refinement of the superstructure shows that both of the analogous octahedra [Mn(2) and Mn(5) in Table 8] are larger. The larger sites in romanechite are located at the edges of the triple chains. Interestingly, the recent refinement of the [2  $\times$  5] structure (Tamada and Yamamoto, 1986) and a Rietveld refinement of todorokite (Post and Bish, 1988) have shown the largest octahedra to be those at the edges of the quintuple chain or triple chains, respectively. It is therefore expected that for the series of related man-

ganese oxide tunnel structures, an analogous segregation of the lower-valence cation will occur. Given the larger size of the Mn(2) octahedra, it is also likely that the larger divalent cations (e.g., Cu<sup>2+</sup>, Zn<sup>2+</sup>, Ni<sup>2+</sup>) are also present in this site in agreement with predictions of Burns et al. (1983, 1985).

The nature of the lower-valence Mn cation can be elucidated through comparison of apical and equatorial Mn–O bond distances in manganese oxides (Table 8). An Mn<sup>3+</sup> octahedron is enlarged in the apical direction by Jahn-Teller distortion, whereas an Mn<sup>2+</sup> octahedron has more equidimensional bond lengths. This distortion is evident from comparison of the apical and equatorial Mn–O bond distances of groutite and manganite (Table 8), which are manganese oxide tunnel structures with essentially only Mn<sup>3+</sup> in the octahedral site. The average apical and equatorial bond lengths for the Mn(2) site of Wadsley's refinement are approximately equal—in fact, the equatorial distance is larger. Our refinement of the substructure, however, shows the average apical distance to be 2.056(6) Å vs. 1.916(4) Å for the equatorial bond distances. The superstructure Mn(2) and Mn(5) sites show similar distortion. This strongly suggests that Mn<sup>3+</sup> is the reduced Mn cation in romanechite. The bond distances for the Mn(3) octahedron in the [2  $\times$  5] structure of Tamada and Yamamoto (1986) show an even greater distortion with an average apical distance of 2.296(13) Å vs. 1.946(9) Å for the equatorial direction. This increased distortion reflects the greater occupancy of this site by Mn<sup>3+</sup> (0.95) in the [2  $\times$  5] structure vs. the ideal occupancy of 0.67 in the Mn(2) site of romanechite. The presence of Mn<sup>3+</sup> in the related manganese oxide tunnel structures is also to be expected. However, for double-chain structures greater than [2  $\times$  5], the Mn<sup>3+</sup> must also occupy a site other than at the edge octahedra of the largest tunnel side, assuming a proportional increase of tunnel cations.

TABLE 4. Selected bond lengths (Å) for romanechite substructure

Mn(1)–O(1)	1.918(6) $\times$ 2	O(1)–O(2)	2.801(7) $\times$ 2
–O(5)	1.904(4) $\times$ 4	–O(4)	2.552(8)
Mean	1.909(5)	–O(5)	2.807(8) $\times$ 2
Mn(2)–O(1)	1.935(4) $\times$ 2	–O(5)'	2.594(7) $\times$ 2
–O(2)	1.933(6)	O(2)–O(3)	2.518(8)
–O(4)	1.896(4) $\times$ 2	–O(3)'	2.771(7) $\times$ 2
–O(5)	2.118(7)	–O(4)	2.754(7) $\times$ 2
Mean	1.962(5)	–O(4)'	2.896(7) $\times$ 2
Mn(3)–O(2)	1.870(4) $\times$ 2	O(3)–O(3)	2.525(6) $\times$ 2
–O(3)	1.921(6)	–O(4)	2.711(7) $\times$ 2
–O(3)'	1.933(4) $\times$ 2	O(4)–O(5)	2.919(8) $\times$ 2
–O(4)	1.899(6)	O(5)–O(5)	2.53(1)
Mean	1.904(5)		
Ba(1)–O(1)	2.943(6) $\times$ 2	O(6)–O(1)	2.97(3) $\times$ 2
–O(2)	3.640(6)	–O(2)	3.61(3)
–O(3)	2.992(5) $\times$ 2	–O(3)	2.93(2) $\times$ 2
–O(4)	3.149(6)	–O(4)	3.07(3)
–O(5)	2.942(6) $\times$ 2	–O(5)	2.92(3) $\times$ 2
–O(5)'	3.005(7)	–O(5)'	3.08(3)

#### Distortions and shifts in the subcell

Difference-Fourier maps of the substructure atoms show small electron-density peaks over several of the framework-atom positions that may be related to problems in the absorption correction. However, some atoms show

TABLE 5. Romanechite superstructure atom positions, temperature factors, and occupancies

Atom	X	Y	Z	U <sup>a</sup>	Occ <sup>**</sup>	U <sub>11</sub> †	U <sub>22</sub> †	U <sub>33</sub> †	U <sub>12</sub> †	U <sub>13</sub> †	U <sub>23</sub> †
Mn(1)	0	½	0	102(15)		160(28)	21(20)	108(25)	0	34(20)	0
Mn(2)	0.9993(2)	0	0.2690(3)	88(9)		151(18)	36(15)	79(16)	0	29(14)	0
Mn(3)	0.3405(2)	0	0.4846(3)	84(8)		130(17)	39(12)	85(15)	0	11(13)	0
Mn(4)	0	0.1668(5)	0	96(8)		183(16)	25(11)	89(13)	0	45(11)	0
Mn(5)	0.5000(1)	0.1665(3)	0.2678(2)	85(5)		127(9)	35(8)	93(9)	-12(9)	0(7)	4(9)
Mn(6)	0.8398(1)	0.1666(2)	0.4839(2)	93(5)		135(9)	36(7)	103(9)	-7(9)	22(7)	5(8)
O(1)	0.567(1)	0	0.177(2)	131(47)		157(90)	98(91)	184(88)	0	-30(68)	0
O(2)	0.098(1)	0	0.426(2)	132(50)		307(109)	39(81)	66(72)	0	-72(73)	0
O(3)‡	0.766(1)	0	0.392(2)	84(39)		87(78)	0(48)	117(80)	0	-4(62)	0
O(4)	0.426(1)	0	0.337(2)	79(47)		36(73)	52(86)	159(85)	0	35(59)	0
O(5)	0.925(1)	0	0.068(2)	176(56)		341(110)	39(92)	183(86)	0	82(71)	0
O(6)	0.0670(6)	0.166(2)	0.1776(9)	103(25)		187(50)	30(44)	98(41)	0(60)	67(35)	-18(51)
O(7)	0.5975(6)	0.167(2)	0.4234(9)	113(26)		121(45)	70(47)	170(45)	-11(56)	16(37)	47(56)
O(8)	0.2664(7)	0.166(1)	0.3978(9)	129(25)		198(52)	118(36)	89(47)	-34(62)	19(38)	53(49)
O(9)	0.9244(7)	0.166(2)	0.334(1)	134(30)		213(54)	68(50)	107(44)	31(59)	46(37)	67(61)
O(10)	0.4271(7)	0.168(2)	0.075(1)	177(32)		147(48)	83(53)	334(58)	-4(63)	112(39)	35(69)
Ba(1)	0.2455(6)	0	0.1236(7)	129(16)	0.481(6)	191(17)	40(10)	141(20)	0	-33(14)	0
Ba(2)	0.7473(4)	0.1662(9)	0.1243(6)	141(16)	0.258(6)	100(17)	186(25)	114(18)	4(38)	40(12)	-21(38)
O(11)	0.249(7)	0	0.143(8)	§	0.530		Isotropic temperature factor fixed to U = 3.0				
O(12)‡	0.753(3)	0.173(4)	0.129(4)	288(114)	0.749	1576(381)	1(123)	578(218)	-29(261)	-16(148)	-9(197)

<sup>a</sup> Refined isotropic temperature factors from the last cycle before anisotropic refinement.

<sup>\*\*</sup> The sum of the occupancies of Ba(1) and Ba(2) were constrained to microprobe value and total occupancy of each tunnel site [i.e., Ba(1) + O(11) and Ba(2) + O(12)] were constrained to 1.0.

† The coefficients are each × 10<sup>4</sup>.

‡ The temperature factors were nonpositive definite in the previous cycle.

§ Isotropic temperature factor went negative.

split electron density likely related to actual shifts of the atoms. Most prominently, O(5) shows two distinct sites. This atom is one of the apical oxygens for the Mn(2) octahedra and would be expected to occupy two sites, depending upon the presence or absence of Mn<sup>3+</sup>. It is also less constrained than the other apical oxygen [O(2)], allowing for greater movement. This positional disorder is also reflected in the temperature factors for O(5), which are larger than for the other oxygen atoms. Other atoms would also be expected to shift as a result of Mn<sup>3+</sup> occupancy, and in fact, the temperature factors for all of the oxygen atoms are larger than normal for well-ordered structures. Also, it is likely that framework atoms will adjust their positions depending on whether a particular tunnel site is occupied by Ba or H<sub>2</sub>O.

The three Mn sites in romanechite are constrained along *b* by a mirror plane, and Mn(1) is further constrained by a twofold axis. However, the Mn(2) and Mn(3) sites are shifted off the centers of their respective octahedra so as to maximize the distance between them as in hollandite (Post et al., 1982). For example, the adjacent Mn(3) sites are shifted away from one another. Similarly, the Mn(2) sites are shifted away from adjacent Mn(1) sites. These shifts likely minimize energy in the structure by reducing repulsive forces.

### Superstructure

Wadsley (1953) proposed a superstructure for romanechite in which *b* of the subcell is tripled based on the observed 2:1 ratio of H<sub>2</sub>O to Ba (Fig. 3). Our refinement of the superstructure indicates that approximately ⅔ of the Ba is in the Ba(1) site and that most of the water is in the O(12) site, near Ba(2). The superstructure results also suggest that the Ba atoms and water molecules oc-

cupy slightly different positions, perhaps partially explaining the large temperature factor refined for the (Ba,H<sub>2</sub>O) site in the subcell. Note especially the difference in *z* between Ba(1) and O(11) [0.1236(6) vs. 0.143(8), Table 5]. Again, the relatively small U<sub>22</sub> anisotropic temperature factors may reflect a problem with the absorption correction. Correspondingly, the Mn(2) octahedron has a greater Mn–O apical bond distance than does the Mn(5) octahedron, indicating a greater occupancy of Mn<sup>3+</sup> near the tunnel site with a greater occupancy of Ba<sup>2+</sup>. A similar correlation was noted by Tamada and Yamamoto (1986).

A remaining problem is the cause of the streaking of the superstructure reflections along [20 $\bar{1}$ ]\*. Such streaking is due to some type of planar disorder. The refinement confirms that the superstructure reflections arise from ordering of Ba and H<sub>2</sub>O on the tunnel sites. The sharpness of the superstructure "spots" (streaks) in the *b*\* direction indicates that the Ba<sup>2+</sup> and H<sub>2</sub>O are well ordered within individual tunnels. There is also ordering between tunnels, as shown by the sharpness of spots in the [201]\* direction (Fig. 2a). The almost continuous streaking in the [20 $\bar{1}$ ]\* direction, however, indicates only short-range ordering in that direction. Although the nature of this short-range ordering is unknown, it may relate to differences in the [20 $\bar{1}$ ] and [201] resulting from the  $\beta$  angle that is not exactly 90°.

### SUMMARY

Points of interest derived from this work include the following:

1. The refinement of the structure of romanechite has yielded more precise atom positions and bond distances than obtained by the previous refinement of Wadsley

TABLE 7. Selected bond lengths (Å) for romanechite superstructure

Mn(1)–O(1)	1.91(2) × 2	Mn(4)–O(5)	1.90(1) × 2
–O(10)	1.91(1) × 4	–O(6)	1.922(9) × 2
Mean	1.91(1)	–O(10)	1.90(2) × 2
		Mean	1.91(1)
Mn(2)–O(2)	2.01(2)	Mn(5)–O(1)	1.93(1)
–O(5)	2.17(2)	–O(4)	1.90(1)
–O(6)	1.94(1) × 2	–O(6)	1.93(1)
–O(9)	1.89(1) × 2	–O(7)	1.98(1)
Mean	1.97(1)	–O(9)	1.90(1)
		–O(10)	2.09(1)
		Mean	1.96(1)
Mn(3)–O(3)	1.95(2)	Mn(6)–O(2)	1.86(1)
–O(4)	1.89(2)	–O(3)	1.94(1)
–O(7)	1.87(1) × 2	–O(7)	1.88(1)
–O(8)	1.93(1) × 2	–O(8)	1.91(1)
Mean	1.91(1)	–O(8) <sup>y</sup>	1.93(1)
		–O(9)	1.90(1)
		Mean	1.90(1)
O(1)–O(4)	2.56(2)	O(6)–O(6)	2.85(2)
–O(6)	2.84(1) × 2	–O(7)	2.79(2)
–O(7)	2.80(2) × 2	–O(9)	2.55(1)
–O(10)	2.57(2) × 2	–O(10)	2.58(2)
–O(10) <sup>y</sup>	2.82(2) × 2	–O(10) <sup>y</sup>	2.83(2)
O(2)–O(3)	2.52(2)	O(7)–O(7)	2.84(2)
–O(6)	2.82(2) × 2	–O(8)	2.52(2)
–O(7)	2.85(1) × 2	–O(8) <sup>y</sup>	2.77(2)
–O(8)	2.76(2) × 2	–O(9)	2.77(2)
–O(9)	2.75(2) × 2	–O(9) <sup>y</sup>	2.90(2)
–O(9) <sup>y</sup>	2.91(2) × 2		
O(3)–O(7)	2.78(2) × 2	O(8)–O(8)	2.50(1)
–O(8)	2.54(2) × 2	–O(8) <sup>y</sup>	2.83(2)
–O(8) <sup>y</sup>	2.85(1) × 2	–O(9)	2.72(2)
–O(9)	2.70(2) × 2		
O(4)–O(7)	2.75(2) × 2	O(9)–O(9)	2.85(2)
–O(7) <sup>y</sup>	2.88(2) × 2	–O(10)	2.89(2)
–O(8)	2.72(2) × 2		
–O(9)	2.84(2) × 2		
–O(10)	2.92(2) × 2		
O(5)–O(5)	2.53(3)	O(10)–O(10)	2.54(2)
–O(6)	2.63(2) × 2	–O(10) <sup>y</sup>	2.85(2)
–O(6) <sup>y</sup>	2.78(2) × 2		
–O(9)	2.95(2) × 2		
–O(10)	2.84(2) × 2		
Ba(1)–O(2)	3.64(2)	O(11)–O(4)	3.1(1)
–O(4)	3.17(2)	–O(5)	3.0(1)
–O(5)	2.96(2)	–O(6)	3.0(1) × 2
–O(6)	2.93(1) × 2	–O(8)	3.0(1) × 2
–O(8)	2.99(1) × 2	–O(10)	2.9(1) × 2
–O(10)	2.96(1) × 2	–O(12)	2.80(4) × 2
–O(12)	2.80(4) × 2	–O(12) <sup>y</sup>	2.9(1) × 2
–O(12) <sup>y</sup>	2.91(4) × 2		
Ba(2)–O(1)	2.95(2)	O(12)–O(1)	3.03(5)
–O(3)	2.96(2)	–O(3)	2.90(4)
–O(5)	2.92(2)	–O(5)	2.90(5)
–O(6)	2.95(1)	–O(7)	3.62(5)
–O(7)	3.64(1)	–O(9)	3.01(5)
–O(8)	3.02(1)	–O(10)	2.86(5)
–O(9)	3.14(1)	–O(10) <sup>y</sup>	3.16(5)
–O(10)	2.94(1)	–O(12)	2.90(6)
–O(10) <sup>y</sup>	3.03(1)	–O(12) <sup>y</sup>	2.95(5)
–O(11)	2.8(1)		
–O(11) <sup>y</sup>	2.850(9)		
–O(12)	2.84(4)		
–O(12) <sup>y</sup>	2.90(4)		

TABLE 8. Comparison of manganese–oxygen bond lengths (Å) for various manganese oxide tunnel structures

Material	Average bond distance			Reference
	Octahedral	Apical	Equatorial	
Pyrolusite	1.8857(2)	1.8981(3)	1.8795(2)	Baur (1976)
Hollandite*				Post et al. (1982)
Mn(1)	1.925(1)	1.932(2)	1.921(1)	
Mn(2)	1.926(1)	1.934(2)	1.922(1)	
Cryptomelane*				Post et al. (1982)
Mn(1)	1.917(1)	1.927(2)	1.912(1)	
Mn(2)	1.918(1)	1.928(2)	1.913(1)	
Romanechite (substructure)				Wadsley (1953)
Mn(1)	1.92	1.85	1.95	
Mn(2)**	1.99	1.97	2.00	
Mn(3)†	1.90	1.89	1.90	
Romanechite (substructure)				this work
Mn(1)	1.909(5)	1.918(6)	1.904(5)	
Mn(2)**	1.962(5)	2.056(6)	1.916(4)	
Mn(3)†	1.904(5)	1.910(6)	1.902(4)	
Romanechite (superstructure)				this work
Mn(1)	1.91(1)	1.91(2)	1.91(2)	
Mn(2)**	1.97(1)	2.09(2)	1.92(1)	
Mn(3)†	1.91(1)	1.92(2)	1.90(1)	
Mn(4)	1.91(2)	1.922(9)	1.90(2)	
Mn(5)**	1.96(1)	2.04(1)	1.92(1)	
Mn(6)†	1.90(1)	1.90(1)	1.90(1)	
Synthetic 2 × 5 structure				Tamada and Yamamoto (1986)
Mn(1)	1.930(10)	1.921(14)	1.935(9)	
Mn(2)	1.937(11)	1.948(13)	1.932(10)	
Mn(3)**	2.063(10)	2.296(13)	1.946(9)	
Mn(4)†	1.946(11)	1.930(14)	1.954(9)	
Manganite	2.038(19)	2.267(25)	1.923(16)	Dachs (1963)
Groutite	2.041(3)	2.259(3)	1.932(3)	Dent Glasser and Ingram (1968)

\* Hollandite and cryptomelane also have Fe in the octahedral sites.  
 \*\* Octahedra are at the end of the largest side of structure (triple or quintuple chain side).

† Octahedra are on the double-chain side of structures.

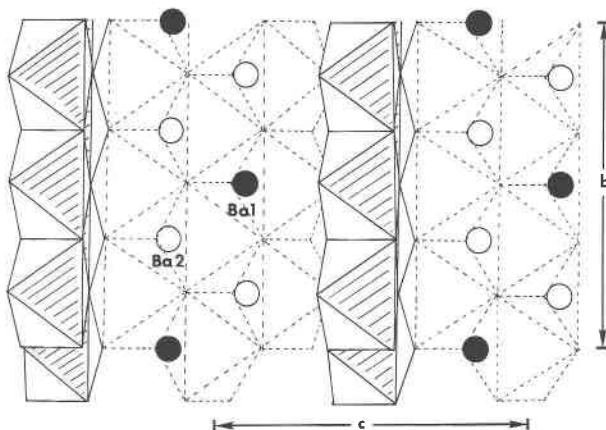


Fig. 3. Projection of the romanechite structure down *a* (assuming  $\beta = 90^\circ$ ). The arrangement of tunnel cations and water gives rise to the superstructure (tripling along *b*) with Ba ordering into Ba(1) and H<sub>2</sub>O into Ba(2) sites.

(1953) and consequently provides a more detailed understanding of the structure.

2. Jahn-Teller distortion of the Mn(2) octahedron strongly suggests that Mn<sup>3+</sup> is the lower-valence Mn cation and that it is ordered into the Mn(2) site. This result is consistent with studies of todorokite and Rb<sub>0.27</sub>MnO<sub>2</sub>.

3. Supercell reflections on long-exposure X-ray diffrac-

tion patterns and our structure refinement indicate an ordering of Ba and H<sub>2</sub>O in the tunnel direction. Strengthening of the supercell reflections indicates disordering of Ba and H<sub>2</sub>O between tunnels in one direction.

## ACKNOWLEDGMENTS

We appreciate helpful discussions with Daniel Appleman and the technical support of Daphne Ross and Jim Collins. Joseph Nelen performed the water analyses. Reviews of this paper by David Bish, Roger Burns, Peter Buseck, and Alan Mighell are appreciated.

## REFERENCES CITED

- Baur, W.H. (1976) Rutile-type compounds. V. Refinement of  $\text{MnO}_2$  and  $\text{MgF}_2$ . *Acta Crystallographica*, B32, 2200–2204.
- Burnham, C.W. (1966) Computation of absorption corrections, and the significance of end effect. *American Mineralogist*, 51, 159–167.
- Burns, R.G., Burns, V.M., and Stockman, H.W. (1983) A review of the todorokite-buserite problem: Implications to the mineralogy of marine manganese nodules. *American Mineralogist*, 68, 972–980.
- (1985) The todorokite-buserite problem: Further considerations. *American Mineralogist*, 70, 205–208.
- Chukhrov, F.V., Gorshkov, A.I., Dmitrieva, M.T., and Svitsov, A.V. (1983) Crystallochemical features of romanechite. *Izvestia Akademii Nauk, Seriya Geologicheskaya*, 83, no. 3, 68–75.
- Dachs, H. (1963) Neutronen- und Röntgenuntersuchungen am Maganit,  $\text{MnOOH}$ . *Zeitschrift für Kristallographie*, 118, 303–326.
- Dent Glasser, L.S., and Ingram, L. (1968) Refinement of the crystal structure of groutite,  $\alpha\text{-MnOOH}$ . *Acta Crystallographica*, B24, 1233–1236.
- Giovanoli, R., and Balmer, B. (1983) Darstellung und Reaktionen von Psilomelan (Romanechit)  $\text{Ba}_2\text{Mn}_3\text{O}_{30} \cdot 4\text{H}_2\text{O}$ . *Chimia*, 37, no. 11, 424–427.
- International Tables for X-ray Crystallography. (1974) Vol. 4, Kynoch Press, Birmingham.
- Mukherjee, B. (1965) Crystallography of psilomelan,  $\text{A}_3\text{X}_2\text{Mn}_8\text{O}_{16}$ . *Mineralogical Magazine*, 35, 643–655.
- Post, J.E., and Bish, D.L. (1988) Rietveld refinement of the todorokite structure. *American Mineralogist*, 73, 861–869.
- Post, J.E., Von Dreele, R.B., and Buseck, P.R. (1982) Symmetry and cation displacements in hollandites: Structure refinements of hollandite, cryptomelane and priderite. *Acta Crystallographica*, B38, 1056–1065.
- Shannon, R.D. (1976) Revised effective ionic radii and systematic studies of interatomic distances in halides and chalcogenides. *Acta Crystallographica*, A32, 751–767.
- Stewart, J.M. (1976) The X-ray system of crystallographic programs. University of Maryland, Technical Report TR-445. College Park, Maryland.
- Tamada, O., and Yamamoto, N. (1986) The crystal structure of a new manganese dioxide ( $\text{Rb}_{0.27}\text{MnO}_2$ ) with a giant tunnel. *Mineralogical Journal*, 13, no. 3, 130–140.
- Turner, S., and Buseck, P.R. (1979) Manganese oxide tunnel structures and their intergrowths. *Science*, 203, 456–458.
- (1981) Todorokites: A new family of naturally occurring manganese oxides. *Science*, 212, 1024–1027.
- Wadsley, A.D. (1953) The crystal structure of psilomelan,  $(\text{Ba},\text{H}_2\text{O})_2\text{Mn}_3\text{O}_{10}$ . *Acta Crystallographica*, 6, 433–438.
- Yanchuk, E.A. (1973) The valency state of manganese in some natural oxides and hydroxides. *Cryptomelane, hollandite, coronadite. Mineralogicheskii Sbornik (Lvov)*, 27, 26–38.
- Yanchuk, E.A., and Povarennykh, A.S. (1975) The valency state of manganese in some natural oxides and hydroxides. *Romanechite. Mineralogicheskii Sbornik (Lvov)*, 29, 9–21.

MANUSCRIPT RECEIVED NOVEMBER 13, 1987

MANUSCRIPT ACCEPTED MAY 20, 1988